HYDROLOGICAL CYCLE IN THE GENERAL CIRCULATION MODEL OF THE MARTIAN ATMOSPHERE

D. S. Shaposhnikov, *Moscow Institute of Physics and Technology, Moscow, Russia (shaposhnikov@phystech.edu)*, **A. V. Rodin**, *Moscow Institute of Physics and Technology, Space Research Institute of Russian Academy of Sciences, Moscow, Russia*, **A. S. Medvedev**, **P. Hartogh**, *Max Planck Institute for Solar System Research, Katlenburg-Lindau, Germany*.

Introduction:

The water cycle plays a significant role in the Martian climate, mostly manifested through radiative effects of water ice clouds. Water vapor can be a very sensitive marker of transport processes, able to challenge 3D climate models.

The history of water cycle implementation in Martian global circulation models (GCMs) starts from the investigation of *Richardson and Wilson* [2002]. Later, the cycle including advection, sublimation and microphysical processes was described in detail by *Montmessin et al.* [2004]. Currently, there are several models of sufficient complexity developed in the United States, France, Great Britain, Japan, Canada and Germany. They are used to study a wide range of processes and phenomena in the atmosphere of Mars as well as for the interpretation of observations. However, the water cycle is reproduced to the most satisfactory extent by the Laboratoire de Météorologie Dynamique (LMD) MGCM [*Montmessin et al.*, 2004; *Navarro et al.*, 2014] and Oxford University MGCM [*Steele et al.*, 2014], which share physical parameterizations.

We present a newly developed hydrological block of the global circulation model developed in Max Planck Institute for Solar System Research and Moscow Institute of Physics and Technology (MPI-MGCM) also known as MAOAM (Martian Atmosphere: Observation and Modeling). The model has a spectral core and successfully predicts the circulation and temperature. It employs physical parameterizations suitable for Martian models, e.g. heating/cooling due to radiative effects of dust, due to IR radiative transfer in CO_2 15 molecules (LTE and non-LTE), gravity waves, etc. [*Hartogh et al.*, 2005, 2007; *Medvedev et al.*, 2000, 2007, 2011, 2015; *Kutepov et al.*, 1998]. The hydrological block to be presented here includes a realistic two-moment microphysics, advection, and sedimentation according to particle sizes.

The model successfully reproduces seasonal variations of water vapor, in both latitude and longitude. We employed Mars Express/SPICAM-IR nadir dataset [*Trokhimovskiy et al.*, 2015] collected during Martian years 27–31 for comparison with the GCM. More detailed consideration of the water vapor geographical distribution shows discrete peaks in longitude during the aphelion season at L_s=90–150°.

Hydrological block description:

Calculation Grid. The MGCM uses a time-evolving pressure grid in vertical parameterized via the hybrid η coordinate [*Simmons and Burridge*, 1981] divided into 50 levels. In horizontal, physics is calculated on the Gauss-Kruger map projection with 32 and 64 bins in latitude and longitude, respectively. This discretization corresponds to a T21 spectral truncation.

Advective transport. The three-dimensional semi-Lagrangian advection employs an explicit monotone second-order hybrid scheme developed in the Polar Geophysical Institute (PGI RAS) and a splitting method in spatial directions [*Mingalev et al.*, 2010].

Diffusion. The importance of vertical turbulent diffusion or eddy mixing for modeling the water cycle was emphasized by *Richardson and Wilson* [2002]. We obtained the best agreement with the experimental data using a simple Crank-Nicolson implicit method with the constant coefficient equal to $10\ m^2 s^{-1}$ for vertical diffusion equation.

Particle bins. The hydrological cycle includes the transport of water vapor and ice particles, the sizes of which are subdivided into bins. Each bin has its own size of dust condensation nuclei. We use 4 bins with radii 0.1, 0.5, 1, 5 μm. A two-moment scheme is used for every bin while maintaining separately the ice mass and number of particles [*Rodin*, 2002].

Sedimentation. The corrections for vertical velocities for every particle bin are calculated according to the equation obtained by *Korablev et al.* [1993] with the Cunningham correction. The correction depends on the effective radius of the bin.

Dust Distribution. We are using a predetermined full dust opacities proposed by *Montmessan et al.* [2004]. Having the dust opacity in the column, the number of dust particles in every bin can be prescribed from log-normal dust distribution obtained by *Fedorova et al.* [2014] using $0.8\ \mu m$ for the effective radius and 0.35 for the effective variance.

Saturation. The water vapor saturation in the atmosphere parcel provides the information about the water amount that the parcel holds. The water vapor saturation pressure on Mars as a function of temperature is expressed through a modification of the August-Roche-Magnus formula [*Curry and Webster*, 1998].

Nucleation. Water ice clouds are formed when water vapor nucleates on dust particles, on so-called cloud condensation nuclei (CCN). In our earlier version [*Shaposhnikov et al.*, 2015], the cloud scheme was rather simple: water vapor is turned instantaneously into ice (or vice versa) reaching the saturation pressure, the number of ice particles was ignored. Now, as was mentioned, it uses a two-moment scheme with 4 bins for different mean nuclei core sizes. For water ice condensing on dust nuclei, we require a heterogeneous nucleation rate. For this, we obtain the homogeneous (without aid of a pre-existing surfaces) homomolecular (nucleation of high molecular weight) nucleation rate first, and then relate it to its heterogeneous counterpart [*Jacobson*, 2005]. The number of active CCN also depends on a parameter $m_h = \cos\theta$, where θ is a "contact angle" (for the liquid phase, it is the angle of the interface between the droplet and its nucleus). We use $m_h = 0.95$ that is consistent with the typical range for Martian dust between 0.97 and 0.93 [*Trainer et al.*, 2008]. There are indications that the value of this parameter influences significantly affects the distribution of water [*Navarro et al.*, 2014].

Particle Growth. Once the ice has condensed, the particles are prone to growth based on various factors. Then the rate of growth is a function of the current water vapor saturation ratio, the saturation pressure ratio over a curved surface, the molecular diffusion resistance and the heat [*Montmessin et al.*, 2002].

Sublimation. The water cycle is fed from water sublimating from the surface. The mechanism that maintains the sublimation is based on the turbulent flux of water at the bottom of the atmosphere [*Montmessin et al.*, 2004].

Results:

The multi-year simulations with the previous version [*Shaposhnikov et al.*, 2015] have been used as an initial condition. Then, the model was run for a Martian year, and data from the second year of simulation are analyzed and presented in the figures below.

Figure 1 illustrates the comparison of the simulated annual water cycle on Mars with the SPICAM. It is seen that the model reproduces both the seasonal asymmetry of the cycle and the general amount of water vapor in the atmosphere. The differences do not exceed 10 p.p.m. and depend on the season. There is a maximum of clouds near the North Pole between L_s=90° and 140°, the characteristic tail directed to the south and the second maximum near 200–230°. Some excess of the vapor amount in the season 170–180° at 0-45°N can be explained by too strong turbulent diffusion and the fact that the SPICAM data were interpolated over 5 Martian years (MY 27-31) with very different conditions. The other problem is the insufficient amount of model vapor at the season L_s 270°. Near the South Pole, this can be caused by the restriction on the surface temperature. We assume that, in the nearest to the South Pole points (south of 85°S), the CO_2 ice is presented permanently on the surface, so that the surface temperature here cannot exceed the CO_2 evaporation temperature. In the middle latitudes, the water scarcity can be caused by the insufficiently accurate dust scenario. Despite the mentioned shortcomings, the simulated cycle has been significantly improved compared to the previous model versions [*Shaposhnikov et al.*, 2016].

Conclusion:

We described the recent version of the hydrological block of the MPI-MGCM. The new block includes a real two-moment microphysics, transport, 4 different sizes of ice particles, condensation, sublimation and sedimentation according to the average radius of particles, the surface microphysics. The simulations have been compared with 10 Earth years of SPICAM (MY 27-31) observations. The comparison shows a good agreement between the observed and simulated water vapor distributions. The MGCM reproduces the distribution and abundances of precipitable water vapor.

The results of simulations can be seen in more detail, plotted and/or downloaded from the site mars.mipt.ru.

Acknowledgments:

We gratefully acknowledge Anna Fedorova, Alexander Trokhimovskiy and Takeshi Kuroda for the assistance with the observational data.

This work was performed at the Laboratory of Applied Infrared Spectroscopy of Moscow Institute of Physics and Technology and supported by the Russian Science Foundation grant 100027.07.32.RSF27.

References:

Curry, J. A., and P. J. Webster (1998), Thermodynamics of atmospheres and oceans, vol. 65, Academic Press.

Fedorova, A., F. Montmessin, A. Rodin, O. Korablev, A. Määattänen, L. Maltagliati, and J.-L. Bertaux (2014), Evidence for a bimodal size distribution for the suspended aerosol particles on mars, Icarus, 231, 239–260.

Hartogh, P., A. S. Medvedev, T. Kuroda, R. Saito, G. Villanueva, A. G. Feofilov, A. A. Kutepov, and U. Berger (2005), Description and climatology of a new general circulation model of the Martian atmosphere, Journal of Geophysical Research: Planets, 110(E11).

Hartogh, P., A. S. Medvedev, and C. Jarchow (2007), Middle atmosphere polar warmings on Mars: Simulations and study on the validation with sub-millimeter observations, Planetary and Space Science, 55(9), 1103–1112.

Jacobson, M. Z. (2005), Fundamentals of atmospheric modeling, Cambridge University press.

Korablev, O., V. Krasnopolsky, A. Rodin, and E. Chassefiere (1993), Vertical structure of Martian dust measured by Solar infrared occultations from the Phobos spacecraft, Icarus, 102(1), 76–87.

Kutepov, A., O. Gusev, and V. Ogibalov (1998), Solution of the non-lte problem for molecular gas in planetary atmospheres: Superiority of accelerated lambda iteration, Journal of Quantitative Spectroscopy and Radiative Transfer, 60(2), 199–220.

Medvedev, A. S., G. P. Klaassen (2000), Parameterization of gravity wave momentum deposition based on nonlinear wave interactions: basic formulation and sensitivity tests, J. Atmos. Solar-Terr., 62, 1015-1033.

Medvedev, A. S., and P. Hartogh (2007), Winter polar warmings and the meridional transport on Mars simulated with a general circulation model, Icarus, 186(1), 97–110.

Medvedev, A. S., E. Yiğit, P. Hartogh, and E. Becker (2011), Influence of gravity waves on the Martian atmosphere: General circulation modeling, Journal of Geophysical Research: Planets, 116(E10).

Medvedev, A. S., F. Gonzalez-Galindo, E. Yiğit, A. G. Feofilov, F. Forget, and P. Hartogh (2015), Cooling of the Martian thermosphere by CO2 radiation and gravity waves: An intercomparison study with two general circulation models, Journal of Geophysical Research Planets, 120, 913-927.

Mingalev, V., I. Mingalev, O. Mingalev, A. M. Oparin, and K. Orlov (2010), Generalization of the hybrid monotone second-order finite difference scheme for gas dynamics equations to the case of unstructured 3d grid, Computational Mathematics and Mathematical Physics, 50(5), 877–889.

Montmessin, F., P. Rannou, and M. Cabane (2002), New insights into Martian dust distribution and water-ice cloud microphysics, Journal of Geophysical Research: Planets (1991–2012), 107(E6), 4–1.

Montmessin, F., F. Forget, P. Rannou, M. Cabane, and R. Haberle (2004), Origin and role of water ice clouds in the Martian water cycle as inferred from a general circulation model, Journal of Geophysical Research: Planets, 109(E10).

Navarro, T., J.-B. Madeleine, F. Forget, A. Spiga, E. Millour, F. Montmessin, and A. Määttänen (2014), Global climate modeling of the Martian water cycle with improved microphysics and radiatively active water ice clouds, Journal of Geophysical Research: Planets, 119(7), 1479–1495.

Richardson, M. I., and R. J. Wilson (2002), Investigation of the nature and stability of the Martian seasonal water cycle with a general circulation model, Journal of Geophysical Research: Planets, 107(E5).

Rodin, A. (2002), On the moment method for the modeling of cloud microphysics in rarefied turbulent atmospheres: I. condensation and mixing, Solar System Research, 36(2), 97–106.

Shaposhnikov, D., A. Rodin, and A. Medvedev (2016), The water cycle in the general circulation model of the Martian atmosphere, Solar System Research, 50(2), 90–101.

Simmons, A. J., and D. M. Burridge (1981), An energy and angular-momentum conserving vertical finite-difference scheme and hybrid vertical coordinates, Monthly Weather Review, 109(4), 758–766.

Steele, L. J., S. R. Lewis, M. R. Patel, F. Montmessin, F. Forget, and M. D. Smith (2014), The seasonal cycle of water vapour on Mars from assimilation of thermal emission spectrometer data, Icarus, 237, 97–115.

Trainer, M. G., O. B. Toon, and M. A. Tolbert (2008), Measurements of depositional ice nucleation on insoluble substrates at low temperatures: Implications for Earth and Mars, The Journal of Physical Chemistry C, 113(6), 2036–2040.

Trokhimovskiy, A., A. Fedorova, O. Korablev, F. Montmessin, J.-L. Bertaux, A. Rodin, and M. D. Smith (2015), Mars' water vapor mapping by the SPICAM IR spectrometer: Five Martian years of observations, Icarus, 251, 50–64.

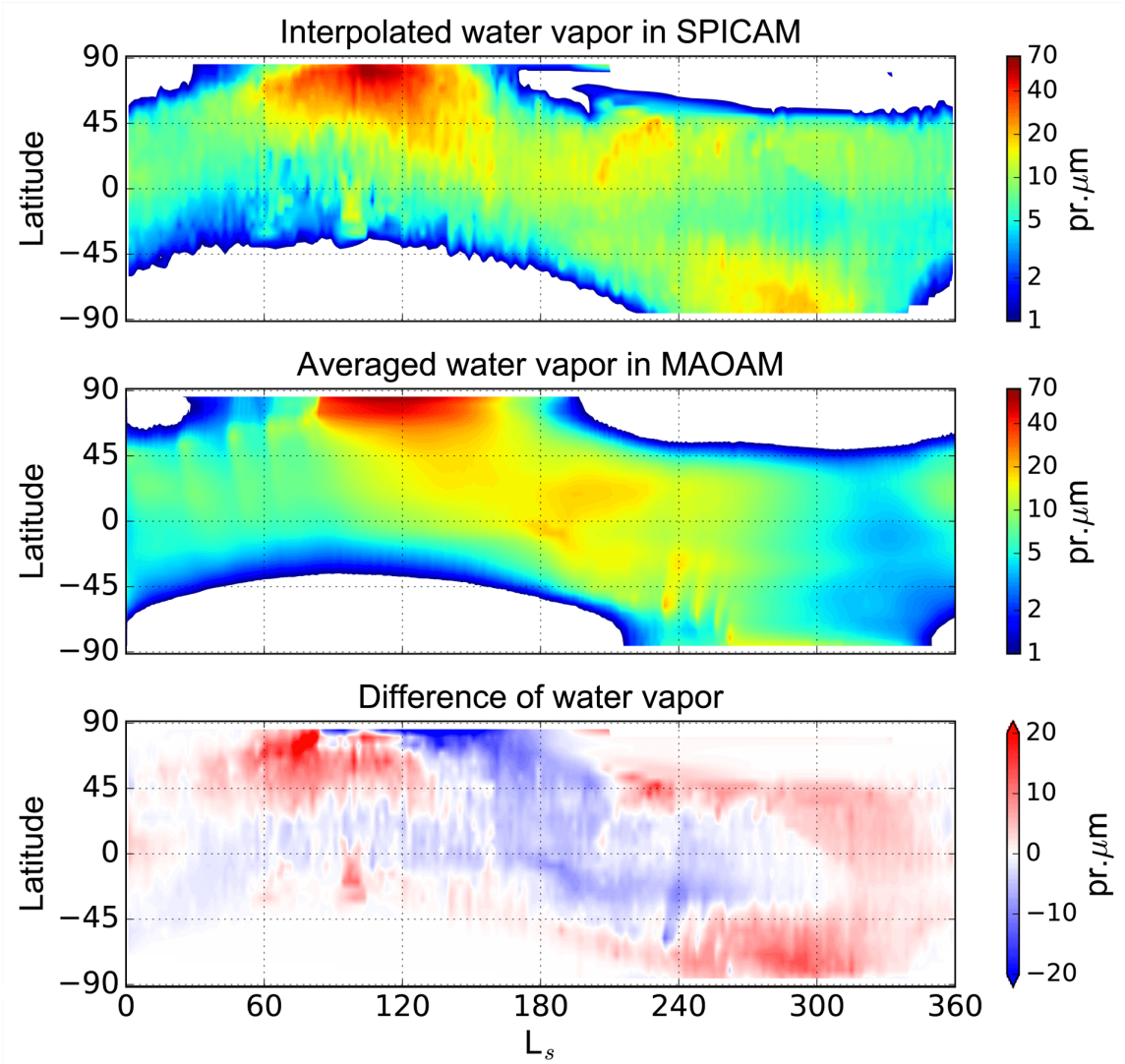

Fig. 1. The comparison of the annual water cycle on Mars according to SPICAM data [*Trokhimovskiy et al.*, 2015] and the GCM. The first image shows precipitable water vapor from SPICAM averaged over 5 Martian years 27–31 and longitudes and then interpolated on the regular grid. The next picture displays the same for GCM data. The last picture illustrates the difference between SPICAM data and our model. Horizontal axis is one Martian year in L_s. Vertical axis is latitude.